Photochemistry and Photobiology, 2014, 90: 997–1003

Photophysical Properties and Singlet Oxygen Generation Efficiencies of Water-Soluble Fullerene Nanoparticles

Alexander S. Stasheuski[1], Victor A. Galievsky[1], Alexander P. Stupak[1], Boris M. Dzhagarov[1], Mi Jin Choi[2], Bong Hyun Chung[2] and Jin Young Jeong*[2]

[1]B.I. Stepanov Institute of Physics, National Academy of Sciences of Belarus, Minsk, Belarus
[2]BioNanotechnology Research Center, Korea Research Institute of Bioscience and Biotechnology, Daejeon, South Korea

Received 15 April 2014, accepted 27 May 2014, DOI: 10.1111/php.12294

ABSTRACT

As various fullerene derivatives have been developed, it is necessary to explore their photophysical properties for potential use in photoelectronics and medicine. Here, we address the photophysical properties of newly synthesized water-soluble fullerene-based nanoparticles and polyhydroxylated fullerene as a representative water-soluble fullerene derivative. They show broad emission band arising from a wide-range of excitation energies. It is attributed to the optical transitions from disorder-induced states, which decay in the nanosecond time range. We determine the kinetic properties of the singlet oxygen ($^1O_2$) luminescence generated by the fullerene nanoparticles and polyhydroxylated fullerene to consider the potential as photodynamic agents. Triplet state decay of the nanoparticles was longer than $^1O_2$ lifetime in water. Singlet oxygen quantum yield of a series of the fullerene nanoparticles is comparably higher ranging from 0.15 to 0.2 than that of polyhydroxylated fullerene, which is about 0.06.

INTRODUCTION

Since its discovery in 1985, buckminsterfullerene (C_{60}) has stimulated a large body of research due to its unique photophysical properties (1–4). Although the fluorescence of C_{60} is intrinsically week, chemical modification allows C_{60} to raise its fluorescence (3,4). Moreover, the color of fullerene nanoparticles may be tuned by varying the C_{60} concentration in the reaction solution (5). In general, certain carbon nanomaterials exhibit optical emission due to quantum confinement effects (6). In this way, nanosized carbon materials have attracted much attention as they are expected to replace conventional cadmium-based quantum dots. Triplet state properties of modified C_{60} should also be promising, as pristine fullerene readily generates singlet oxygen ($^1O_2$) and other reactive oxygen species by illuminating ultraviolet or visible light (7,8). Energy transfer from the excited triplet state of fullerene to the ground state of oxygen gives rise to $^1O_2$ as illustrated in the following scheme:

$$\text{fullerene} + h\nu \rightarrow {}^1\text{fullerene}^* \quad (1)$$

$${}^1\text{fullerene}^* \rightarrow {}^3\text{fullerene}^* \quad (2)$$

$${}^3\text{fullerene}^* + {}^3O_2 \rightarrow \text{fullerene} + {}^1O_2 \quad (3)$$

Singlet oxygen is able to irreversibly cause damage of various cellular organelles and biomolecules, including mitochondria, lipid, and nucleus, thus leading to damage of target diseased cells or tissue (9). Photosensitizer, a generator of singlet oxygen by irradiating light, is an important factor in photodynamic therapy. Although C_{60}-fullerene is known to be a strong singlet oxygen generator (singlet oxygen generation quantum yield is 1), it has been limitedly used in photodynamic therapy due to its extremely low solubility in water. To overcome this drawback, many efforts have been explored to develop the water-soluble C_{60} by various approaches including reaction with hydrophilic moieties, grafting polymers, and applying surfactants (10). As a rule, such modification of C_{60} significantly affects its photophysical properties. For example, fullerol ($C_{60}(OH)_{24}$), a representative water-soluble fullerene, is known to have low efficiency of $^1O_2$ generation compared to that of pristine fullerene (11). Therefore, it is a challenge to synthesize water-soluble fullerene derivatives with sufficient photosensitizing activity.

Recently, highly water-soluble fullerene nanoparticles (C_{60}-TEGs) were prepared by conjugating C_{60} with tetraethylene glycol (TEG) using lithium hydroxide as a catalyst (Fig. 1) (5).

In current work, we investigated the photophysical properties of the C_{60}-TEGs including time-resolved fluorescence, triplet state lifetime, and singlet oxygen generation quantum yield by combining various experimental approaches of conventional and time-resolved spectroscopy. In particular, we compared the photophysical properties of these new water-soluble fullerene nanoparticles with that of a representative water-soluble fullerene (polyhydroxylfullerene ($C_{60}(OH)_n$)) by measuring the $^1O_2$ kinetic luminescence signals to demonstrate the potential of C_{60}-TEGs as a photosensitizer.

MATERIALS AND METHODS

Materials. Bukminsterfullerene (C_{60}) and polyhydroxylfullerene ($C_{60}(OH)_n$) were obtained from MER Co. (AZ, USA). Tetraethylene glycol

*Corresponding author email: jyjeong@kribb.re.kr (Jin Young Jeong)

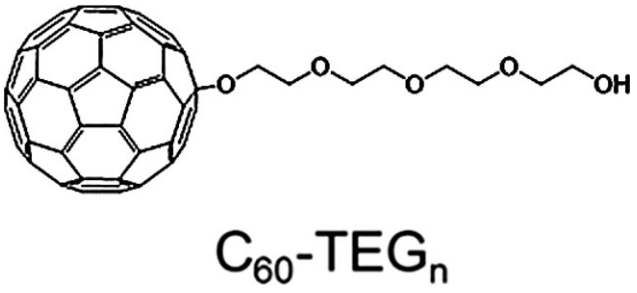

Figure 1. Structure of tetraethyleneglycol-conjugated fullerene (C_{60}-TEG_n).

and lithium hydroxide were purchased from Sigma–Aldrich (St. Louis, MO, USA). 5,10,15,20-Tetrakis(N-methyl-4-pyridyl)-21H,23H-porphine (TMPyP) tosylate salt was kindly provided by Dr. V.L. Malinovskii.

Synthesis of water-soluble fullerene nanoparticles. The water-soluble fullerene nanoparticles were prepared following previous procedure (5). Five mL of fullerene dissolved in toluene with various concentrations (0.12, 0.25, 0.5, 1.0, 2.0 mg mL^{-1}) was mixed with 5 mL of tetraethylene glycol. Then, 20 mg of lithium hydroxide was added to the mixture solution, and the solution was stirred for 20 h at room temperature. After stirring, the mixture solutions were precipitated by adding excess of ethyl acetate and redissolved in ethanol. This step was repeated at least three times to remove the unreacted chemicals. The precipitates (C_{60}-TEGs) were finally dried by evaporation and kept in storage until use. The nanoparticles were denoted as CT006, CT012, CT025, CT050, and CT100, according to initially used fullerene concentration in toluene/tetraethylene glycol mixture (0.06, 0.12, 0.25, 0.5, and 1.0 mg mL^{-1} ,respectively). The chemical characteristics of the fullerene nanoparticles were analyzed by FTIR, XPS, and NMR methods, and the results were similar to those previously reported. The analysis revealed that a large fraction of C_{60} is oxidized inside of the nanoparticles. During preparation, the concentration of C_{60} was the main factor in controlling the size and chemical composition of the C_{60}-TEGs. Increasing initial concentration of C_{60} yielded the fullerene nanoparticles of greater size and correspondingly mass.

Steady-state absorption and fluorescence measurements. Absorption spectra were recorded on an MC 122 spectrophotometer (Proscan Special Instruments, Belarus) in quartz cuvettes. Fluorescence emission and excitation spectra were recorded on a CM 2203 spectrofluorimeter (SOLAR, Belarus) using the excitation wavelength at 350 nm and the emission wavelength at 550 nm, respectively. The fluorescence quantum yield, φ, was determined by a relative method using a solution of quinine sulfate in 1.0 *N* H_2SO_4 as a fluorescent standard, for which the quantum yield of 0.546 was obtained (12). The relative accuracy in determination of the φ values was 10%.

Time-resolved fluorescence measurements. The lifetimes of the excited singlet state, τ_1 and τ_2, of the fullerene derivatives were determined by measuring fluorescence decays using a modified PRA-3000 pulse fluorometer (Photochemical Research Associates, Canada) operating in the time-correlated single photon counting mode. The excitation source was a 378-nm pulsed light-emitting diode (PLS-380, PicoQuant GmbH, Germany), full width at half maximum (FWHM) of the diode pulses being ~990 ps. The decays were analyzed by means of Edinburgh FLA900 software. The values of τ_i were determined by the nonlinear least-squares reconvolution analysis of fluorescence decay curves assuming a double-exponential fluorescence decay law $F(t) = F_1\exp(-t/\tau_1) + F_2\exp(-t/\tau_2)$. The estimated relative errors in fluorescence lifetimes were about 5%.

Flash photolysis. Triplet state decay traces were recorded using a home-made laser transient absorption setup (13). The excitation light source was a LS-2134 Nd:YAG laser (JV LOTIS TII, Belarus) providing 355 nm pulses of 15 ns FWHM and 1 mJ energy. A 150 W xenon arc lamp (OSRAM AG, Germany) was used as a probe beam. Detection of the signal in the visible region was performed with a FEU-128 photomultiplier tube via an MS2004i monochromator (SOLAR TII Ltd., Belarus). The C_{60}-TEG solutions were prepared with optical densities of the samples about 0.4 at the excitation wavelength. To evaluate triplet state lifetime, τ_T, signals were fitted by exponential decay function.

Singlet oxygen luminescence measurement. The luminescence of singlet oxygen was measured using a modified laser near-infrared lifetime spectrometer (detection range 950–1400 nm), which was created at the Institute of Physics of the National Academy of Sciences of Belarus (14,15). Samples were excited by the third harmonic (355 nm) of an Nd:YAG laser (LS-2134, JV LOTIS TII, Belarus). Typical parameters of the laser were as follows: the pulse width of 15 ns, the pulse energy of 20 μJ, and the repetition rate of 15 Hz. Luminescence radiation, collected with a high-throughput optical system, was spectrally isolated with an MS2004i monochromator (SOLAR TII Ltd., Belarus) and directed to a photomultiplier tube (model H10330-45, Hamamatsu Photonics K.K.), operated in the photon-counting mode. After amplification by C5594-44 unit (Hamamatsu Photonics K.K.), the output of the photomultiplier tube was sent to a multiscaler (P7888-2, FAST ComTec GmbH). The time channel width of the multiscaler was set to 32 ns. Singlet oxygen quantum yield, γ_Δ, is a ratio of number of produced singlet oxygen molecules to the number of absorbed quanta of excitation light by sensitizer molecules. The most common method of γ_Δ estimation is a comparative one. To evaluate γ_Δ from the C_{60}-TEGs, we compared intensities of near-infrared (~1270 nm) luminescence of $^1O_2$ generated by the C_{60}-TEGs and the TMPyP in water, the latter being a standard (16) with $\gamma_\Delta^{st} = 0.77 \pm 0.04$.

The common expression for the time dependence of the number of $^1O_2$ molecules may be derived under condition of pulsed laser excitation of the photosensitizer (17–20):

$$[^1O_2](t) = \frac{\gamma_\Delta N_L(1 - 10^{-OD})\tau_\Delta}{\tau_\Delta - \tau_T} \cdot \{\exp(-t/\tau_\Delta) - \exp(-t/\tau_T)\} \tag{4}$$

where $[^1O_2]$ is the concentration of singlet oxygen molecules, γ_Δ is the singlet oxygen quantum yield, N_L is the number of quanta in the laser pulse, *OD* is the optical densities of the solute at the excitation wavelength, τ_Δ and τ_T are lifetimes of singlet oxygen and photosensitizer triplet state, respectively.

The intensity of $^1O_2$ emission is proportional to the concentration of produced $^1O_2$ molecules (19,20):

$$I(t) = \frac{\alpha k_r}{n^2}[^1O_2](t) = I_0\frac{\tau_\Delta}{\tau_\Delta - \tau_T} \cdot \{\exp(-t/\tau_\Delta) - \exp(-t/\tau_T)\} \tag{5}$$

where α is a constant that contains geometrical and electronic factors of the detection system, k_r is $^1O_2$ radiative decay constant, n is the solvent refractive index,

$$I_0 = \alpha k_r \gamma_\Delta N_L(1 - 10^{-OD})/n^2 \tag{6}$$

Equation (6) may be used to determine singlet oxygen quantum yields. Under the identical experimental conditions the γ_Δ from the modified fullerenes was calculated according to:

$$\gamma_\Delta = \gamma_\Delta^{st} \cdot \frac{I_0}{I_0^{st}} \cdot \frac{(1 - 10^{-OD})^{st}}{(1 - 10^{-OD})} \tag{7}$$

In Eq. (7), the superscript "*st*" corresponds to the standard.

To observe singlet oxygen luminescence, optical densities of both standard and investigated samples were ~0.2 at 355 nm excitation wavelengths. To minimize samples photodegradation, continuous magnetic stirring was used. Within the signal accumulation time, the optical density of all samples decreased no more than by 5%. Average values of optical densities were used to calculate singlet oxygen quantum yields.

RESULTS AND DISCUSSION

Absorption and fluorescence characteristics

We have employed two different fullerene derivatives: (i) $C_{60}(OH)_n$, a covalent functionalized hydroxylated C_{60}, and (ii) the C_{60}-TEGs particles. Both of these fullerene derivatives are readily soluble in water. However, it has been reported that some

functionalized fullerenes may form aggregates in polar media at high concentrations (11,21,22). To verify the formation of aggregates, UV-visible absorption spectra of different concentrations of the C_{60}-TEGs and $C_{60}(OH)_n$ in aqueous solution were recorded. As shown in Fig. 2, the absorption of $C_{60}(OH)_n$ in water showed a linear increase at 355 nm with increasing concentration up to 58 μM (Fig. 2A, inset). The same linear tendency is observed for the CT006 (Fig. 2B, inset) and for other C_{60}-TEGs (not shown). For the separate sample, all normalized absorption spectra were coincided with each other. These results clearly showed that in aqueous solution both $C_{60}(OH)_n$ molecules and the C_{60}-TEGs particles were present in the monomeric state.

Previously, for the $C_{60}(OH)_{24}$ and $C_{60}(OH)_{36}$, deviation from the Beer-Lambert law was observed at micromolar concentrations and above (11,22), when the $C_{60}(OH)_{24}$ and $C_{60}(OH)_{36}$ became aggregated, possibly due to the formation of a hydrogen bond network. In present work, $C_{60}(OH)_n$ was supplied by MER Co in the form of a salt with the following stochiometric formula: $C_{60}(OH)_x(ONa)_y$, with x + y = 24 and y around 6–10. Thus, 24 carbon atoms are hydroxylated in our compound. The discrepancy between results of different scientific groups may be explained by the nature of hydroxylated fullerene. Synthetic routes in the works (11,22) may result in large number of OH-groups readily forming hydrogen bonds in water solutions, whereas our samples bear at least six repulsing O^- group on their surface.

The broad absorption spectra extended up to 800 nm (Fig. 3) indicate the absence of a well-defined bandedge in the UV-vis energy range both for the C_{60}-TEGs and $C_{60}(OH)_n$.

In contrast to the broad absorption features, relatively narrow fluorescent peaks (FWHM ~ 0.7 eV) centered around 580 nm are observed. Fluorescent spectra of both the C_{60}-TEGs and $C_{60}(OH)_n$ possess near-Gaussian shape, slight asymmetry being introduced by little shoulders. The fluorescent quantum yield of $C_{60}(OH)_n$ is about 0.3%, while for the C_{60}-TEGs the largest ϕ is about 1% as found previously (5).

The fluorescent excitation spectra obtained in the maximum of the emission spectrum agree well with the corresponding absorption spectra of the C_{60}-TEGs and $C_{60}(OH)_n$. However, the fluorescent excitation spectra obtained for different wavelengths of the emission spectrum ranging from 430 to 660 nm slightly differ in shape between each other. The longer detection wavelength is used, the more excitation spectrum is shifted to "red" region. Also the fluorescence spectra undergo insignificant "red" shift, when excitation wavelength is increased from 290 to 450 nm. All these little differences in wavelength-dependent excitation and emission spectra are caused by small heterogeneity of particles' size, confirming SEM measurements performed in (5). Therefore, each studied species actually possesses one dominant type of fluorophores.

Figure 3 shows the absence of mirror symmetry between the absorption and fluorescent emission spectra. And this fact cannot be accounted by the small heterogeneity of nanoparticles' size. Thorough analysis of experimental papers concerning carbon materials provides a number of luminescent nano-objects, which do not show mirror symmetry between excitation and emission luminescence spectra: graphene oxide (23), reduced graphene oxide (24), and graphene quantum dots (25). Although much progress has been achieved in graphene-related studies, the origin of the fluorescence of modified graphene is still a controversial

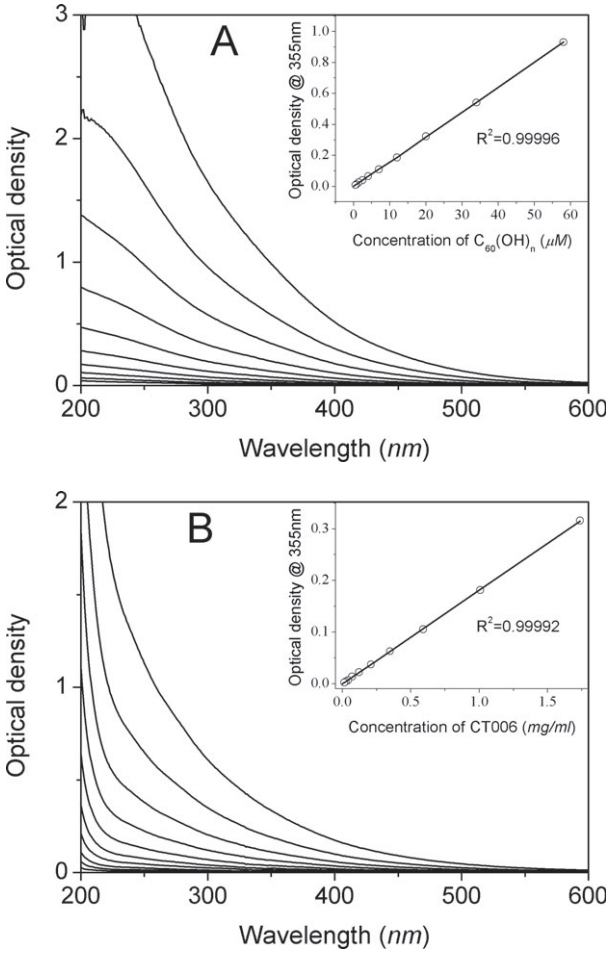

Figure 2. UV-vis absorption spectra of different concentrations of $C_{60}(OH)_n$ (A) and CT006 (B) in aqueous solution. Spectra from bottom to top correspond to [$C_{60}(OH)_n$] 0.5, 0.8, 1.4, 2.4, 4.0, 7.0, 12, 20, 34, 58 μM and [CT006] 0.01, 0.02, 0.04, 0.07, 0.12, 0.21, 0.35, 0.59, 1.0, 1.7 mg mL^{-1}. Insets: Plots of the absorbance at 355 nm against the concentration; path length, 1 cm.

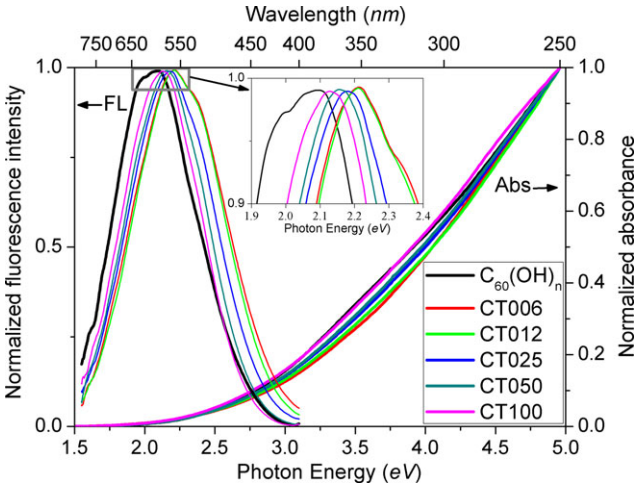

Figure 3. Normalized fluorescent and absorption spectra of the C_{60}TEGs and $C_{60}(OH)_n$ water solutions. The fluorescent spectra were obtained for excitation at 350 nm (3.54 eV).

issue with variety of models and theories (23). As discussed in *Experimental* section, the core of the C_{60}-TEGs consists of conjugated fullerene molecules. So, the fullerene core of the studied particles brings together the C_{60}-TEGs with fullerene films (26), carbon nanodots (27), and graphite nanoparticles, obtained by transformation of C_{60} molecules (28). At the same time, fullerene molecules are chemically modified by oxygen and TEG residuals on the surface of the C_{60}-TEGs.

Chemical bonds of C_{60} with carbon, oxygen and hydrogen introduce sp^3 hybridized sites into a sea of sp^2 hybridized carbon of pristine fullerene. Therefore, the C_{60}-TEGs may be similar to hydrogenated amorphous carbon (29) and to chemically derived graphene oxide (24), which contain both sp^3 and sp^2 sites. As was shown earlier (5), a large fraction (30–40%) of aromatic carbon in C_{60}-TEGs is sp^3 hybridized and covalently bonded with oxygen in form of epoxy and hydroxyl groups similar to graphene oxide (30). The remaining aromatic carbon is sp^2 hybridized and bonded either with neighboring carbon atoms or with oxygen in the form of ketone group.

In carbon materials, containing a mixture of sp^3 and sp^2 bonding, the σ bonds of sp^3 and sp^2 sites give rise to σ valence and σ^* conduction-band states (31). The π and π^* states of the sp^2 sites lie within the σ–σ^* gap, and form the band edges and control the optical gap. Because of (i) the large energy difference between sp^2 and sp^3 sites and (ii) their disorder localization in the C_{60}-TEGs, these particles may be treated just like conventional amorphous semiconductors, with disorder-induced states (32). As a result, in presented fullerene materials broad emission band arising from a wide range of excitation energies (Fig. 3) may be mainly attributed to optical transitions from these disorder-induced states (Fig. 4).

As mentioned above, in amorphous semiconductors, sp^2 sites control the optical gap. Robertson deduced empirical linear dependence between photoluminescence energy and sp^2 carbon fraction for different samples of hydrogenated amorphous carbon (29). It is known that carbon can form double bonds with itself and different heteroatoms. This requires sp^2 hybridization of its valence atomic orbitals. Based on the relative content of C=C and C=O bonding as measure of sp^2 carbon inside the C_{60}-TEGs (5), we obtain good linear relationship with maxima of fluorescence spectra of the particles, as shown in Fig. 5.

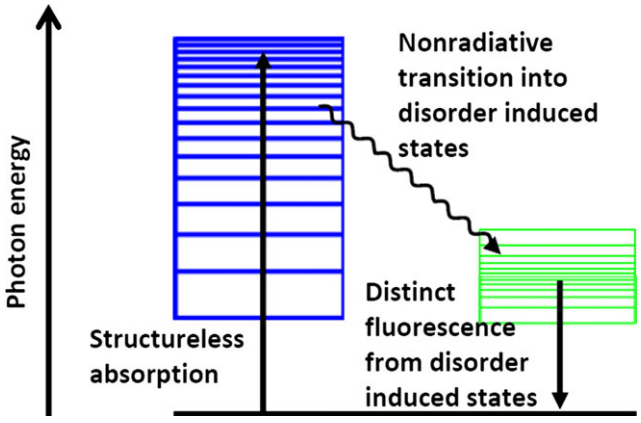

Figure 4. Schematic diagram showing the origin of emission in C_{60}-TEGs from disorder-induced states.

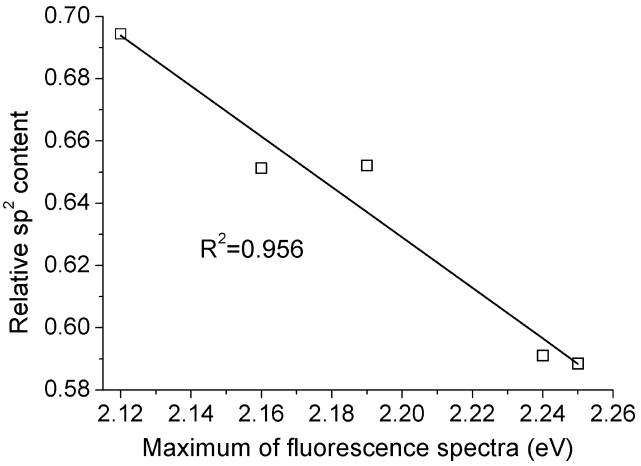

Figure 5. Relative content of C=C and C=O bonding in the C_{60}TEGs *versus* maxima of fluorescence spectrum of these particles.

Table 1. Summary of lifetimes and weighting factors*, WF_i, from double-exponential fitting of fluorescence decay kinetics.

Sample	τ_1, ns	WF_1	τ_2, ns	WF_2
CT006	1.2	0.45	4.2	0.55
CT012	1.1	0.44	4.1	0.56
CT025	1.2	0.50	4.2	0.50
CT050	0.9	0.43	3.3	0.57
CT100	1.1	0.49	3.5	0.51
$C_{60}(OH)_n$	0.8	0.50	3.6	0.50

*Weighting factors were calculated as $WF_i = F_i\tau_i/(F_1\tau_1 + F_2\tau_2)$.

To understand better the fluorescent behavior of the different C_{60}-TEGs particles and the $C_{60}(OH)_n$, time-resolved photoluminescence decay were monitored at 550 nm, using 378 nm as excitation wavelength. Each decay curve was fitted to the double-exponential function (Table 1), resulting in a fast component (~1 ns) and a slow one (~4 ns). Inherently, disorder-induced states are a set of separate states (32). They may be treated as a set of separate fluorophores, which both decay nonradiative and emit light with different rates. Therefore, double-exponential law to describe fluorescence of the C_{60}-TEGs particles is a simplification and results listed in Table 1 may be used only to compare different samples between each other.

The samples with red shifted fluorescent spectra (Fig. 3) emit light faster than the particles with blue shifted fluorescent spectra. However, for all samples contribution of fast decay component is almost equal to the slow one.

Triplet state properties

While the large body of calculations and measurements of optical properties of nanoparticles (23–25,27,29,31–33), the nature of the optically active states has remained controversial. Both fluorescence and phosphorescence of nanoparticles may be used in a variety of applications (34). Moreover, diatomic oxygen is able to quench nanoparticle's triplet states resulting in formation of singlet oxygen, which is the main cytotoxic agent during photodynamic therapy of malignant tumors (9). Therefore, nanoparticles with long-lived triplet state are promising for medical treatment and diagnostics. Flash photolysis experiments resulted

Table 2. Lifetimes of triplet state of investigated sensitizers; lifetimes and quantum yields of singlet oxygen sensitized by the standard porphyrin and by the modified fullerenes in air equilibrated distilled water solutions.

Sample	τ_T*, μs	τ_T†, μs	T_Δ, μs	γ_Δ
TMPyP	1.9 ± 0.1	1.8 ± 0.1	3.7 ± 0.1	0.77
CT006	9.0 ± 1.2	13 ± 1	1.9 ± 0.4	0.16 ± 0.03
CT012	9.2 ± 1.1	11 ± 1	2.5 ± 0.4	0.15 ± 0.02
CT025	9.3 ± 1.7	11 ± 1	1.7 ± 0.4	0.18 ± 0.03
CT050	7.1 ± 0.8	10 ± 1	2.3 ± 0.3	0.20 ± 0.03
CT100	7.0 ± 1.4	8.9 ± 0.9	2.3 ± 0.4	0.19 ± 0.03
$C_{60}(OH)_n$	5.9 ± 1.3	6.2 ± 1.5	1.6 ± 0.8	0.06 ± 0.02

*During flash photolysis, triplet state decay was monitored at 600 nm.
†Triplet state lifetimes, obtained from measurements of singlet oxygen luminescence. Confidence intervals for all values are stated at the 80% confidence level.

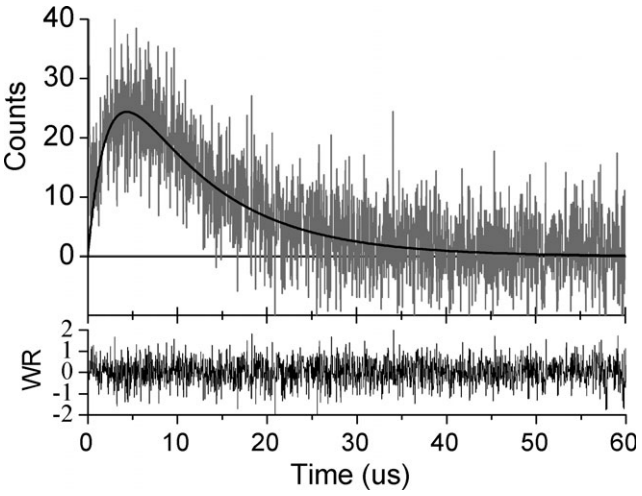

Figure 6. Kinetics of CT050-photosensitized luminescence of singlet oxygen in water at excitation wavelength 355 nm after 7.5×10^3 laser pulses. The time resolution is 32 ns channel^{-1}. The average noise level equal to 80 counts was subtracted from the signal. A solid line is the two-exponential curve fitting by Eq. (5). $^1O_2$ luminescence rise and decay times were found to be 2.3 ± 0.3 μs and 10 ± 1 μs, respectively. WR are the weighted residuals.

in longer triplet state lifetime for the modified fullerenes than for the porphyrin (Table 2). As mentioned in previous section, disorder-induced states may be treated as a set of separate fluorophores. Triplet state lifetime is *a priori* longer than singlet state lifetime and collisions with molecular oxygen define decay of triplet states in most cases. Therefore, conventionally different disorder-induced states inside separate particle possess the same triplet state lifetime resulting in mono exponential triplet decay (Table 2).

It is known that oxygen quenching of sensitizer triplet states is mainly governed by diffusion-controlled bimolecular collisions and spin-statistical factor (35). The corresponding rate constant for quenching of the triplet state lies near 10^9 m^{-1}s^{-1}. Taking into account, the concentration of molecular oxygen in water ($3 \cdot 10^{-4}$ m), the typical triplet-state lifetime of water-soluble sensitizers is about 2–3 μs (14,18,20,36–38). As we can see from the Table 2, in comparison with the porphyrin, the C_{60}-TEGs and $C_{60}(OH)_n$ are effectively shielded from the interaction with ground state oxygen. TEG residues at the C_{60}-TEG particle's outer layer protect sufficiently excited triplet state from dissolved oxygen quenching. Also OH surface groups shield fullerene core of both the C_{60}-TEGs and $C_{60}(OH)_n$. Similar shielding effect was found for the number of fulleropyrrolidine and bismethanofullerenedendrimers in aerated organic solvents (3). It was proofed that dendritic wedges are able to protect fullerene cores from the quenching of oxygen molecules.

Singlet oxygen generation efficiency

In most pure solvents under 1 atm. pressure due to high concentration and diffusion rate of dissolved oxygen, triplet state lifetime is generally much shorter than singlet oxygen lifetime. Therefore, the rising part of $^1O_2$ signal from Eq. (5) is described by τ_T and the decay part by τ_Δ. But if the sensitizer is effectively shielded from interaction with ground state oxygen, τ_T may become larger than τ_Δ. Consequently, denominator in Eq. (5) will be negative leading to $\tau_{rise} = \tau_\Delta$ and $\tau_{decay} = \tau_T$ which is so called inversion of kinetic phases in detected signal (18,36). As was mentioned above, the modified fullerenes are effectively shielded from interaction with ground state oxygen. Therefore, when illuminated by UV light, the C_{60}-TEGs and $C_{60}(OH)_n$ produce clear kinetic signal of $^1O_2$ luminescence at 1270 nm with inverted kinetic phases (Table 2, Fig. 6). Similar effect was observed for chlorin e_6 binding with polyvinylpyrrolidone in aqueous solutions (37).

The biexponential fit of TMPyP signal at 1270 nm by Eq. (5) yields $\tau_T \sim 1.8$ μs, being the typical value of triplet state lifetime of this porphyrin (38), and $\tau_\Delta \sim 3.7$ μs corresponding singlet oxygen lifetime in pure water (39–41). There is no literature evidence of time-resolved investigations of the C_{60}-TEGs and $C_{60}(OH)_n$ triplet state or their singlet oxygen generation in water. Data recorded at 1270 nm yielded time constants, τ_Δ (Table 2), being smaller than the typical value 3.7 μs in pure water.

After $^1O_2$ formation, it interacts both with solvent and with the C_{60}-TEGs molecules. Within the accuracy of measurements, rate constants of $^1O_2$ deactivation $k_\Delta = 1/\tau_\Delta \sim (0.5 \pm 0.1)$ μs^{-1} were the same for all C_{60}-TEGs.

Based on FTIR analysis, the C_{60}-TEGs have high density of hydroxyl group (OH) which may act as an effective quencher of singlet oxygen luminescence (42). Moreover, $^1O_2$ in $C_{60}(OH)_n$ water solution has the same rate constants $k_\Delta \sim 0.6$ μs^{-1}similar in the solutions of the fullerene nanoparticles. Therefore, the presence of hydroxyl termini is the reason of faster $^1O_2$ deactivation in solutions under investigation in comparison with water solution of porphyrinoid sensitizer, where singlet oxygen decays with a rate constant about 0.3 μs^{-1}.

Time-resolved luminescence signals at 1270 nm were used to determine the efficiency of singlet oxygen generation by the modified fullerenes (Table 2). Recent years many papers studying phototoxicity of different forms of water-soluble fullerene derivatives have been published (11,22,43,44). In particular, fullerol $C_{60}(OH)_{24}$, has been investigated and its photophysical properties including singlet oxygen generation are studied. Zhao *et al.* (11) reported the γ_Δ of singlet oxygen generation by fullerol as 0.08 in deuterated water at 366 nm excitation wavelength. Kong *et al.* (45) mentioned that the γ_Δ were ranging from 0.048 to 0.1 depending on pH. In this study, we also measured the γ_Δ of polyhydroxylfullerene ($C_{60}(OH)_n$) purchased from MER Corp. to compare its capability of singlet oxygen generation with the

newly synthesized water-soluble fullerene derivatives. The γ_Δ value for $C_{60}(OH)_n$ was equal to 0.06, which was lower than those obtained from the C_{60}-TEGs. Therefore the C_{60}-TEGs more efficiently generate singlet oxygen than polyhydroxylfullerene and fullerol.

CONCLUSIONS

We studied luminescent and photophysical properties of polyhydroxylfullerene and the new C_{60}-TEGs nanoparticles. Broad emission band arising from a wide-range of excitation energies was attributed to optical transitions from disorder-induced states. For all the C_{60}-TEGs particles, nanosecond photoluminescence kinetics does not decay monoexponentially. The fluorescent quantum yield of $C_{60}(OH)_n$ is about 0.3%. For the first time, the $^1O_2$ kinetic luminescence signals produced by polyhydroxylfullerene and the C_{60}-TEGs nanoparticles were detected in water. The kinetic phases of singlet oxygen traces at 1270 nm from the modified fullerenes were inverted as their triplet state lifetimes were longer than singlet oxygen decay. Singlet oxygen quantum yield was obtained up to 0.2 for all the C_{60}-TEGs particles.

Acknowledgements—This work was supported by Belarusian Republican Foundation for Fundamental Research (Grant No. Ph12KOR-002), National Research Foundation of Korea (Grant No. 2012K2A1-A2033135), and the KRIBB Initiative Program.

REFERENCES

1. Arbogast, J. W., A. P. Darmanyan, C. S. Foote, Y. Rubin, F. N. Diederich, M. M. Alvarez, S. J. Anz and R. L. Whetten (1991) Photophysical properties of C_{60}. *J. Phys. Chem.* **95**, 11–12.
2. Terazima, M., N. Hirota, H. Shinohara and Y. Saito (1991) Photothermal investigation of the triplet state of C_{60}. *J. Phys. Chem.* **95**, 9080–9085.
3. Accorsi, G. and N. Armaroli (2010) Taking advantage of the electronic excited states of [60]-fullerenes. *J. Phys. Chem. C* **114**, 1385–1403.
4. Huang, L., X. Cui, B. Therrien and J. Zhao (2013) Energy-funneling-based broadband visible-light-absorbing bodipy–C_{60} triads and tetrads as dual functional heavy-atom-free organic triplet photosensitizers for photocatalytic organic reactions. *Chem. Eur. J.* **19**, 17472–17482.
5. Jeong, J., J. Jung, M. Choi, J. W. Kim, S. J. Chung, S. Lim, H. Lee and B. H. Chung (2012) Color tunable photoluminescent fullerene nanoparticles. *Adv. Mater.* **24**, 1999–2003.
6. Liu, L., S. Ryu, M. R. Tomasik, E. Stolyarova, N. Jung, M. S. Hybertsen, M. L. Steigerwald, L. E. Brus and G. W. Flynn (2008) Graphene oxidation: Thickness-dependent etching and strong chemical doping. *Nano Lett.* **8**, 1965–1970.
7. Tabata, Y. and Y. Ikada (1999) Biological functions of fullerene. *Pure Appl. Chem.* **71**, 2047–2053.
8. Mroz, P., G. P. Tegos, H. Gali, T. Wharton, T. Sarna and M. R. Hamblin (2007) Photodynamic therapy with fullerenes. *Photochem. Photobiol. Sci.* **6**, 1139–1149.
9. Ochsner, M. J. (1997) Photophysical and photobiological processes in photodynamic therapy of tumors. *J. Photochem. Photobiol., B* **39**, 1–18.
10. Markovic, Z. and V. Trajkovic (2008) Biomedical potential of the reactive oxygen species generation and quenching by fullerene (C_{60}). *Biomaterials* **29**, 3561–3573.
11. Zhao, B., Y.-Y. He, P. J. Bilski and C. F. Chignell (2008) Pristine (C_{60}) and hydroxylated [$C_{60}(OH)_{24}$] fullerene phototoxicity towards HaCaT keratinocytes: Type I vs type II mechanisms. *Chem. Res. Toxicol.* **21**, 1056–1063.
12. Demas, J. N. and G. A. Crosby (1971) Measurement of photoluminescence quantum yields – Review. *J. Phys. Chem.* **75**, 991–1024.
13. Chirvony, V. S., I. V. Avilov, A Yu Panarin, V. L. Malinovskii and V. A. Galievsky (2007) The triplet state decay kinetics and deactivation funnel geometry of a series of nonplanar saddle-shaped porphyrins. *Chem. Phys. Lett.* **434**, 116–120.
14. Galievsky, V. A., A. S. Stasheuski, V. V. Kiselyov, A. I. Shabusov, M. V. Belkov and B. M. Dzhagarov (2010) Laser NIR lifetime spectrometer with nanosecond time resolution. *Instrum. Exp. Tech.* **53**, 568–574.
15. Stasheuski, A. S., V. A. Galievsky and B. M. Dzhagarov (2011) Highly sensitive laser spectrometers for near infrared and visible ranges. *Devices and Methods of Measurements: Scientific and Engineering Journal.* **1**, 25–31.
16. Frederiksen, P. K., S. P. McIlroy, C. B. Nielsen, L. Nikolajsen, E. Skovsen, M. Jörgensen, K. V. Mikkelsen and P. R. Ogilby (2005) Two-photon photosensitized production of singlet oxygen in water. *J. Am. Chem. Soc.* **127**, 255–269.
17. Egorov, S. Y., V. F. Kamalov, N. I. Koroteev, A. A. Jr Krasnovsky, B. N. Toleutaev and S. V. Zinukov (1989) Rise and kinetics of photosensitized singlet oxygen luminescence in water. *Chem. Phys. Lett.* **163**, 421–424.
18. Baier, J., T. Fuß, C. Pöllmann, C. Wiesmann, K. Pindl, R. Engl, D. Baumer, M. Maier, M. Landthaler and W. Bäumler (2007) Theoretical and experimental analysis of the luminescence signal of singlet oxygen for different photosensitizers. *J. Photochem. Photobiol., B* **87**, 163–173.
19. Nonell, S. and S. E. Braslavsky (2000) Time-resolved singlet oxygen detection. In *Methods in Enzymology: Singlet Oxygen, UV-A, and Ozone*, Vol. **319** (Edited by L. Packer and H. Sies), pp. 37–49. Academic Press, San Diego.
20. Stasheuski, A. S., V. A. Galievsky, V. N. Knyukshto, R. K. Ghazaryan, A. G. Gyulkhandanyan, G. V. Gyulkhandanyan and B. M. Dzhagarov (2014) Water-soluble pyridyl porphyrins with amphiphilic N-substituents: Fluorescent properties and photosensitized formation of singlet oxygen. *J. Appl. Spectrosc.* **80**, 813–823. (translated from (2013) *Zhurnal Prikladnoi Spektroskopii* **80**, 823–833).
21. Guldi, D. M., H. Hungerbuhler and K. D. Asmus (1995) Unusual redox behavior of a water-soluble malonic-acid derivative of C_{60}: Evidence for possible cluster formation. *J. Phys. Chem.* **99**, 13487–13493.
22. Vileno, B., P. R. Marcoux, M. Lekka, A. Sienkiewicz, T. Fehér and L. Forró (2006) Spectroscopic and photophysical properties of a highly derivatized C_{60} fullerol. *Adv. Funct. Mater.* **16**, 120–128.
23. Shang, J., L. Ma, J. Li, W. Ai, T. Yu and G. G. Gurzadyan (2012) The origin of fluorescence from graphene oxide. *Sci. Rep.* **2**, 1–8.
24. Eda, G., Y.-Y. Lin, C. Mattevi, H. Yamaguchi, H.-A. Chen, I.-S. Chen, C.-W. Chen and M. Chhowalla (2010) Blue photoluminescence from chemically derived graphene oxide. *Adv. Mater.* **22**, 505–509.
25. Liu, F., M.-H. Jang, H. D. Ha, J.-H. Kim, Y.-H. Cho and T. S. Seo (2013) Facile synthetic method for pristine graphene quantum dots and graphene oxide quantum dots: Origin of blue and green luminescence. *Adv. Mater.* **25**, 3657–3662.
26. Benner, R. E., D. Dick, X. Wei, S. Jeglinski, Z. V. Vardeny, D. Moses, V. I. Srdanov and F. Wudl (1994) Optical probes of C_{60} thin films. *Mol. Cryst. Liq. Cryst.* **256**, 241–250.
27. Bao, L., Z.-L. Zhang, Z.-Q. Tian, L. Zhang, C. Liu, Y. Lin, B. Qi and D.-W. Pang (2011) Electrochemical tuning of luminescent carbon nanodots: From preparation to luminescence mechanism. *Adv. Mater.* **23**, 5801–5806.
28. Lu, J., P. S. E. Yeo, C. K. Gan, P. Wu and K. P. Loh (2011) Transforming C60 molecules into graphene quantum dots. *Nat. Nanotechnol.* **6**, 247–252.
29. Robertson, J. (1996) Recombination and photoluminescence mechanism in hydrogenated amorphous carbon. *Phys. Rev. B* **53**, 16302–16305.
30. Yang, D., A. Velamakanni, G. Bozoklu, S. Park, M. Stoller, R. D. Piner, S. Stankovich, I. Jung, D. A. Field, C. A. Jr Ventrice and R. S. Ruoff (2009) Chemical analysis of graphene oxide films after heat and chemical treatments by X-ray photoelectron and Micro-Raman spectroscopy. *Carbon* **47**, 145–152.
31. Robertson, J. and E. P. O'Reilly (1987) Electronic and atomic structure of amorphous carbon. *Phys. Rev. B* **35**, 2946–2957.
32. Taylor, P. C. (2006) The localization of electrons in amorphous semiconductors: A twenty-first century perspective. *J. Non-Cryst. Solids* **352**, 839–850.

33. Efros, A. L., M. Rosen, M. Kuno, M. Nirmal, D. J. Norris and M. G. Bawendi (1996) Band-edge exciton in quantum dots of semiconductors with a degenerate valence band: Dark and bright exciton states. *Phys. Rev. B* **54**, 4843–4856.
34. Sreenivasan, V. K. A., A. V. Zvyagin and E. M. Goldys (2013) Luminescent nanoparticles and their applications in the life sciences. *J. Phys.: Condens. Matter* **25**, 1–23.
35. Dzhagarov, B. M., G. P. Gurinovich, V. E. Novichenkov, K. I. Salokhiddinov, A. M. Shul'ga and V. A. Ganzha (1990) Photosensitized formation of singlet oxygen and the quantum yield of intercombinational transition in porphyrin and metalloporphyrin molecules. *Sov. J. Chem. Phys.* **6**, 2098–2119.
36. Butorina, D. N., A. A. Jr Krasnovsky and A. V. Priezzhev (2003) The kinetic parameters of singlet molecular oxygen in aqueous solutions of porphyrins. dependence on detergents and sodium azide. *Biophysics* **48**, 189–196.
37. Parkhats, M. V., V. A. Galievsky, A. S. Stashevsky, T. V. Trukhacheva and B. M. Dzhagarov (2009) Dynamics and efficiency of the photosensitized singlet oxygen formation by chlorin e6: The effects of the solution pH and polyvinylpyrrolidone. *Opt. Spectrosc.* **107**, 974–980.
38. Kruk, N. N., B. M. Dzhagarov, V. A. Galievsky, V. S. Chirvony and P.-Y. Turpin (1998) Photophysics of the cationic 5,10,15,20-tetrakis (4-N-methylpyridyl) porphyrin bound to DNA, $[poly(dA\text{-}dT)]_2$ and $[poly(dG\text{-}dC)]_2$: Interaction with molecular oxygen studied by porphyrin triplet-triplet absorption and singlet oxygen luminescence. *J. Photochem. Photobiol., B* **42**, 181–190.
39. Rodgers, M. A. J. and P. T. Snowden (1982) Lifetime of $O_2(^1\Delta_g)$ in liquid water as determined by time-resolved infrared luminescence measurements. *J. Am. Chem. Soc.* **104**, 5541–5543.
40. Yegorov, S. Y. and A. A. Jr Krasnovskii (1983) Photosensitized luminescence of oxygen on pulsed laser excitation. Kinetics of decay in aqueous solutions. *Biophysics* **28**, 532–534.
41. Salokhiddinov, K. I., B. M. Dzhagarov and G. D. Egorova (1983) Direct lifetime measurement of molecular oxygen in singlet $^1\Delta_g$ state generated in water by porphyrin-sensitizer. *Opt. Spectrosc.* **55**, 71–73.
42. Schweitzer, C. and R. Schmidt (2003) Physical mechanisms of generation and deactivation of singlet oxygen. *Chem. Rev.* **103**, 1685–1757.
43. Hotze, E. M., A. R. Badireddy, S. Chellam and M. R. Wiesner (2009) Mechanisms of bacteriophage inactivation via singlet oxygen generation in UV illuminated fullerol suspensions. *Environ. Sci. Technol.* **43**, 6639–6645.
44. Krishna, V., A. Singh, P. Sharma, N. Iwakuma, Q. Wang, Q. Zhang, J. Knapik, H. Jiang, S. R. Grobmyer, B. Koopman and B. Moudgil (2010) Polyhydroxy fullerenes for non-invasive cancer imaging and therapy. *Small* **6**, 2236–2241.
45. Kong, L., O. Tendrow, Y. F. Chan and R. Zepp (2009) Light-initiated transformations of fullerenol in aqueous media. *Environ. Sci. Technol.* **43**, 9155–9160.